GANIL

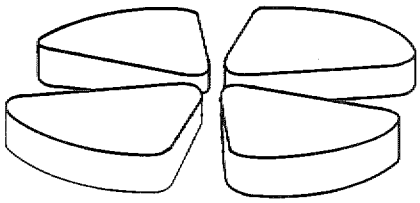

Submitted to NIM B

Neutron production in bombardments of thin and thick W, Hg, Pb targets by 0.4, 0.8, 1.2, 1.8 and 2.5 GeV protons

A.Letourneau, J.Galin,[1] F.Goldenbaum,[2] B.Lott, A.Péghaire

GANIL, IN2P3/CNRS, DSM/CEA, BP5027, F-14076 Caen cedex 05, France

M.Enke, D.Hilscher, U.Jahnke

Hahn Meitner Institut, Glienicker Strasse 100, D-14109 Berlin, Germany

K.Nünighoff, D.Filges, R.D.Neef, N.Paul, H.Schaal, G.Sterzenbach, A.Tietze

Institut für Kernphysik, Forschungzentrum Jülich GmbH, D-52425 Jülich, Germany

GANIL P 00 20

Neutron production in bombardments of thin and thick W, Hg, Pb targets by 0.4, 0.8, 1.2, 1.8 and 2.5 GeV protons

A.Letourneau, J.Galin,[1] F.Goldenbaum,[2] B.Lott, A.Péghaire

GANIL, IN2P3/CNRS, DSM/CEA, BP5027, F-14076 Caen cedex 05, France

M.Enke, D.Hilscher, U.Jahnke

Hahn Meitner Institut, Glienicker Strasse 100, D-14109 Berlin, Germany

K.Nünighoff, D.Filges, R.D.Neef, N.Paul, H.Schaal, G.Sterzenbach, A.Tietze

Institut für Kernphysik, Forschungzentrum Jülich GmbH, D-52425 Jülich, Germany

Abstract

Neutron experimental data relevant to the design of the target of neutron spallation sources are presented and discussed. The data include the reaction cross sections for W, Hg and Pb investigated with 0.4, 0.8, 1.2, 1.8 and 2.5 GeV proton beams as well as the neutron production, neutron multiplicity distribution, as determined event per event using a high efficiency detector. The production as a function of target material is investigated for both thin (with a single reaction) and thick targets (multiple reactions). Comparisons are made with the predictions of a high energy transport code.

PACS numbers : 25.40.Sc, 24.10.-i, 29.25.Dz

Key words: spallation reactions, neutron sources

[1] Corresponding author : Tel.: 33(0)231454574 FAX : 33(0)231454665 E-mail : galin@ganil.fr

[2] Present address : IfK, FZ Jülich

1 INTRODUCTION

With the prospects of building new facilities for high intensity neutron beams for research[1] [2][3], or neutron sources for accelerator-driven transmutation (ADT) of nuclear waste[4][5], both using spallation reactions induced by energetic protons in thick targets, the neutron production in such targets has recently experienced a rising interest. In contrast with older measurements[6][7][8] which only provided average neutron multiplicities, the most recent measurements [9][10][11] have allowed considerable improvement in the available information in so far as they provide the inelastic nuclear reaction probabilities as well as the neutron multiplicity distributions. This is possible thanks to the use of a dedicated tool, well suited for such measurements: a 4π-sr, high efficiency, Gd loaded, liquid scintillator detector[12].

Two series of measurements have already been performed with such an instrument. First, hadron-induced spallation reactions have been investigated at CERN from 2 up to 5 GeV/c for a series of hadrons comprising protons, deuterons, pions of both charges, positive kaons and antiprotons[9][10]. It was shown that the neutron production in thick targets depends primarily on the available energy of the projectile (for antiparticles, the available energy includes the total rest-mass energy in addition to their kinetic energy) but does not depend, to first order, on the nature of the hadron. These data were later complemented at GANIL, at energies up to 200 MeV for protons, deuterons and alpha-particles[11]. At low energy, it was shown how the high electronic stopping power becomes a strong handicap for the neutron production.

Considering a kinetic energy close to 1 GeV as being the most promising for a neutron spallation plant, additional data for energies bracketing this energy are needed in order to improve our knowledge of spallation for potential target materials such as W, Hg and Pb. Moreover and in contrast with previous measurements using secondary beams (except one at 1.22 GeV using protons at the low energy antiproton ring at CERN), the use of a primary beam up to 2.5 GeV at the COSY facility at Jülich has allowed better statistics to be gathered for reaction probabilities, neutron multiplicity distributions and average neutron multiplicities per reaction. Also, in the present work, efficiency corrections for the neutron multiplicity data have been made, taking into account the neutron energy. As it will be shown, these corrections depend on both the target characteristics (nature, size) and on the bombarding energy. The readers interested in the present data with the aim of validating simulation codes will thus find all the material to make a meaningful comparison between experimental data and modeled data. For those readers only interested in the neutron production, the presented data have been fully corrected in order to take into account all biases of experimental origins, in the most accurate way. These data are of great interest for the determination of the neutron

component that contributes to the signal of hadron calorimeters[13].

The experiment was performed on a set of cylindrical targets of different thicknesses and diameters in order to gather data which are relevant for the different steps of the reaction process. The latter consist of the intra-nuclear cascades followed by the deexcitation of the intermediate excited nucleus, in thin targets, whereas the inter-nuclear cascade of secondary particles emitted in a preceding reaction may contribute greatly to the neutron production, as the target thickness increases.

The paper is organized as follows: after a description of the experimental setup in section 2, important features of the data reduction are discussed in sect. 3, before presenting the experimental data in sect. 4 with some comparisons with model calculations. Finally the main results of the experiment are summarized with some prospects for future investigations.

2 EXPERIMENTAL ASPECTS

2.1 Beams and targets

The experiment has been carried out at the COSY accelerator at FZ-Jülich for proton energies of 0.4, 0.8, 1.2, 1.8 and 2.5 GeV. Chemically pure targets of Pb (99.988%) and W (99.98%) were shaped as cylinders whereas the liquid Hg (99.9995%) was encapsulated into 1-mm thick, cylindrical stainless steel containers. The different combinations of beam energy, target material and target size which have been explored are listed in Table 1. The targets were mounted with their symmetry axis aligned on the beam axis. The target volume was limited to cylinders of 15 cm in diameter and 35 cm in length by the available space inside the neutron detector tank. It would have been desirable for the Hg and Pb targets and at high proton energy to explore somewhat more thicker targets but due to its higher density (19.3 g/cm^3 instead of 13.55 and 11.35 g/cm^3 for Hg and Pb, respectively) the use of W has brought a more extended picture of neutron emission as a function of target size within the same available volume.

For orientation, the ranges of the protons are given in Table 2, for the three materials and five bombarding energies, as they would be in absence of nuclear absorption. It can be noted that the 0.4 GeV beam is electronically stopped in all the 35 cm thick targets of W, Hg and Pb, whereas at 1.2 GeV and above the beam can never be electronically stopped in any considered target. At 0.8 GeV the beam is stopped in about 23 cm of W, 34 cm of Hg but not quite in the 35 cm thick Pb target.

Energy		0.4 GeV	0.8 GeV	1.2 GeV	1.8 GeV	2.5 GeV
Target	Diameter	Thickness in cm				
Pb	2 cm	0.5	0.2	0.2	0.2	0.2
	15 cm	5,10,20,35	1,2,5,10,15, 20,25,30,35	1,2,3,5,7, 10,12,15, 20,25,30,35	1,2,3,4,5,7,8, 10,12,15, 20,25,30,35	2,5,10,15,20, 25,30,35
	12 cm	35	1,2,5,10,15, 20,25,30,35	35	15,20,25,30, 35,39	35
	8 cm	1,2,35	1,5,10,15,20, 25,35,40	35	0.5,1,5,10,15, 20,25,30,35 40	2,10,20,35
Hg	2 cm			0.5	0.5	0.5
	15 cm	33.7	2,5,10.23, 15.13,20.23, 25.18,30.45, 33.7	2,3.25,5.23,7, 10.23,15.13, 20.23,25.18, 30.45	2,5,10.23, 15.13,20.23, 25.18,30.45, 33.70	5,10.23,15.13, 20.23,25.18, 30.45,33.70
W	2 cm		0.112	0.112	0.112	0.112
	15 cm	10,20,34.75	2,4,5,7,10,15, 20,25,30, 34.75	1,2,5,10,15, 20,25,30, 34.75	1,2,3,4,5,7, 8,10,12,15, 20,24.74,30, 34.49	1,2,3,5,7,10, 15,20,25,30, 34.75
	12 cm	34.75	34.75	5,20,34.75 34.49	20,24,30,	2,34.75
	8 cm	1,2,34.75	0.5,1,2,3,4,5, 7.5,10,15,20, 25,30,34.75	5,20,34.75	0.5,1,2,3,4,5, 7,10,15,20, 25.2,30.2, 34.49	0.5,2,5,10, 15,25,30, 34.75

Table 1
Different combinations of target materials, target sizes explored at various energies.
Thicknesses are given in cm.

	0.4 GeV	0.8 GeV	1.2 GeV	1.8 GeV	2.5 GeV
Pb	14	40	70	115	170
Hg	12	34	58	96	141
W	8	23	39	66	97

Table 2
Proton ranges (expressed in cm) as they would be in absence of nuclear reactions, as a function of initial energy and target material.

2.2 The 4π neutron detector

The 4π, BNB (Berlin Neutron Ball) detector consists of a spherical shell with outer and inner diameters of 140 and 40 cm, respectively. This 50 cm-thick detector is filled with 1500 l of scintillator liquid loaded with gadolinium (0.3 % in weight). A schematic drawing of the BNB is shown in Fig.1. A nuclear reaction in the target produces a prompt light response in the scintillator, generated by emitted protons, neutrons, pions, γ-rays and eventually a delayed response from Gd-captured neutrons. The light signals are well separated in

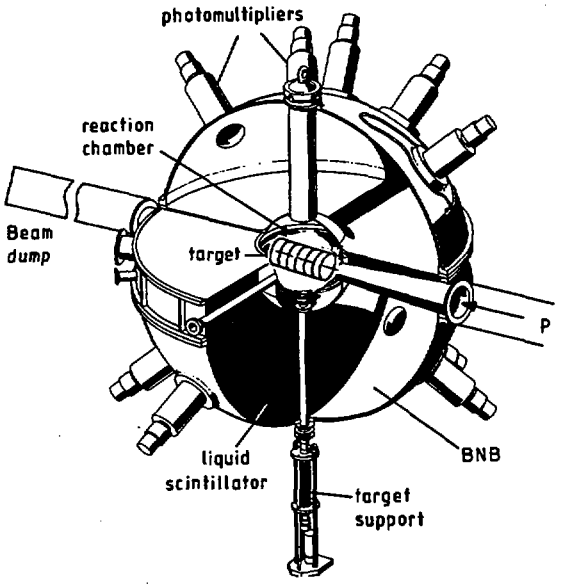

Fig. 1. The 4π Berlin Neutron Ball (BNB) with thick targets stacked in the reaction chamber.

time and this property allows to use the detector in a 2-fold mode. Indeed, the neutrons produced in the target are slowed down by elastic scattering with the H and C atoms of the solvent and are eventually captured at different instants with high cross section by the Gd nuclei when reaching thermal energy. The detector is thus used, first, as a nuclear reaction trigger and then as a neutron multiplicity-meter[14]. The detector response to the γ-rays resulting from the neutron capture is delayed by about 1 to 50 microseconds (about 16 μs on the average) with respect to the reaction. This is mainly due to the low Gd concentration imposing an appreciable diffusion time for the thermalized neutron before being capture by a Gd nucleus. As a consequence, the neutron signals have been selected within a time gate opened 0.7 μs after the reaction takes place and closed after 45 μs when the probability to capture a neutron is reduced to 2%.

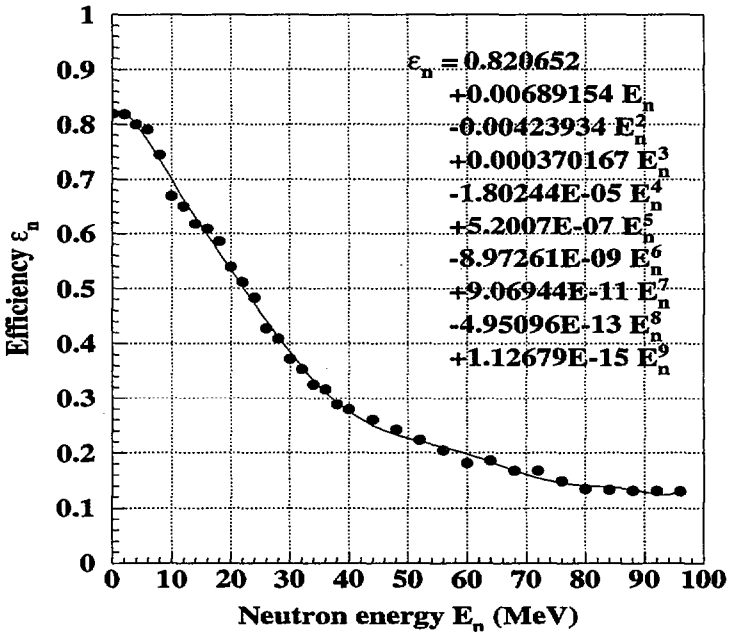

Fig. 2. Detection efficiency of the BNB as a function of neutron energy as calculated with the DENIS code [17] (dots). The data are fitted with the polynomial function as displayed by the solid line (the coefficients of the polynomial are provided).

The scintillator light is registered by 24 fast phototubes distributed evenly at the surface of the tank. It is worth stressing that in contrast with measurements implying liquid scintillator detectors for time-of-flight (TOF) information [15], the present measurements have been performed without low-energy threshold, since the neutron needs to be thermalized anyway (down to 0.025 eV) in order to be captured. The efficiency of the BNB with a 3-fold coincidence between the phototubes, measured to be 82.6% with the $< E >$=2.1 MeV neutrons from a Cf source, remains larger than 55% for neutrons at 20

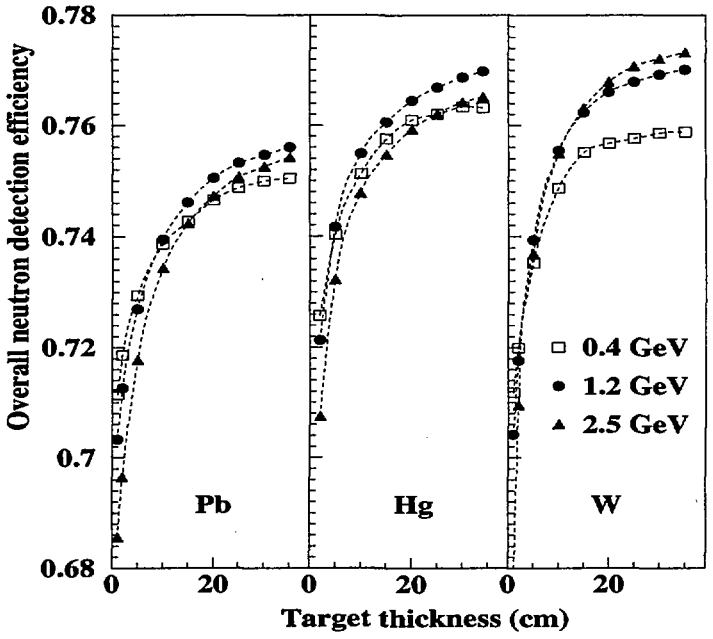

Fig. 3. The overall neutron detection efficiency as simulated for various experimental conditions (for details, see text). All targets are 15 cm in diameter.

MeV, as can be derived from a Monte Carlo simulation[17], and then drops down to about 15% at 100 MeV (Fig.2). The efficiency of the BNB was continuously monitored during the data taking with a Cf source installed on the bottom of the scattering chamber with the neutron counting being triggered and tagged by the detection of a fission fragment. A fit to the BNB efficiency is also given in Fig.2 for a light detection threshold of about 2 MeVee (MeV electron equivalent). The neutrons below 20 MeV are, by far, the most abundant ones emerging from a thin target[15]. The situation is even better, as far as the efficiency is concerned, for neutrons leaking out from thick targets[16], with their much softer kinetic energy spectra. In order to make a reliable efficiency correction for the present measurements, a simulation has been performed, using the HERMES[18] computer code to calculate the kinetic energy distribution of the leaking neutrons and then fold the resulting data with the efficiency of the BNB. The correlation between the neutron kinetic energy and the efficiency is provided by a simulation[17]. The overall efficiency taking into account the neutron energy spectrum for each experimental condition is shown in Fig.3. The detection efficiency increases with increasing target thickness since the leaking neutrons become less and less energetic due to their slowing down within the target. Moreover, with increasing target thickness and material density the high energy spallation neutrons are subject to further nuclear reactions and their energy in the neutron spectrum is thus reduced. The detection efficiency is shown to be excellent in all cases and this makes

the 4π, Gd loaded liquid scintillator detectors unique tools for such measurements. The correction to be applied to the number of observed neutrons is at most 35%. As shown in a previous article[19] for thin targets, this correction depends only very weakly on the INC code (or the parameters therein) used for the simulation. Also, since most of the leaking neutrons have low energy, their detection efficiency can be reliably calibrated with a Cf source. Comparatively, the TOF-type indirect multiplicity measurements[15][16] suffer more drawbacks: a rather high energy threshold preventing the observation of a large fraction of the evaporation neutrons and a low efficiency of the detectors, both intrinsically (since rather thin) and in solid angle.

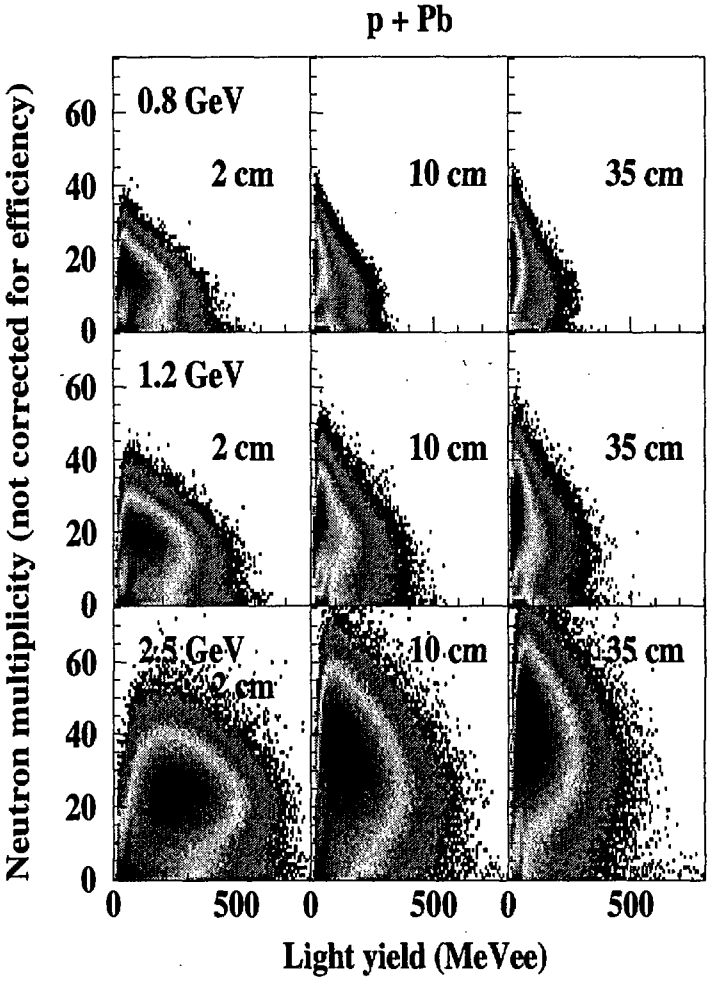

Fig. 4. Distribution of events as a function of the prompt light yield (MeVee) and neutron multiplicity (as measured) in the interaction of 0.8, 1.2, 2.5 GeV protons with 2, 10 and 35 cm thick Pb targets.

The measured neutron multiplicity distributions have been corrected for dead time, correlated and uncorrelated backgrounds. Uncorrelated background, as

measured in presence of beam and absence of target, has been subtracted. The correlated background, measured on-line in a second, 45 μs gate, arbitrarily issued 400 μs after the first counting gate, amounted to less than 0.1 neutron unit on the average. A standard unfolding procedure[12][14] has been applied to correct the data gathered in the first gate, knowing those data recorded in the second gate. The pile-up of 2 neutron captures within the dead time of 35 ns has been corrected for. It amounts to corrections of 1.5, 3.0, 4.8, 8.2 and 12% for 10, 20, 30, 50 and 70 registered neutrons, respectively.

The prompt light signal has been utilized to tag the occurrence of a nuclear reaction. The absolute light yield calibration has been performed with tagged cosmic muons crossing the scintillator tank through its diameter and depositing 190 MeVee. Due to different light conversion efficiencies for different types of particles, the correlation between measured light and neutron multiplicity is quite loose (Fig.4). However, some of the general trends can be understood, at least qualitatively. For instance, for a given target thickness and diameter, one observes on the upper edge of the neutron multiplicity distribution an anticorrelation effect between neutron multiplicity and light yield. This is most likely due to the escaping high-energy particles, baryons and mesons, which generate much more light than evaporated neutrons can do. The less energy these particles are able to lose into the target itself in nuclear reactions, the less they are able to heat up the target nuclei (either in intra- or-inter-nuclear cascades) and the fewer neutrons are evaporated. For a similar reason, the thicker the target, the stronger the prompt light is reduced. For thicker and thicker targets, a larger and larger fraction of the light is generated through the evaporated neutrons and γ-rays. They both suffer a reduction in their energy within the target and the then generated light in the scintillator is small due to the large quenching factor in light production for low-energy neutrons (0.5 MeVee for a 2 MeV neutron). As will be shown later on, the reaction probability as based only on the prompt light measurements can then be somewhat biased for very thick targets.

2.3 The experimental arrangement

The experimental arrangement is sketched in Fig.5. The incoming particles were tagged using a plastic scintillator, S1, 0.3 mm thick, 2 cm in diameter, mounted 2.13 m upstream from the center of the BNB. This signal was used both as a master trigger and a time reference. A set of 5 plastic scintillator detectors S3, S5-S8 located about 1 m in front of the BNB was used as an active collimator for rejecting off-axis incident particles. The adjustable opening of these slits made it easy to define the size of the beam spot on target according to the optical quality of the incoming beam (this was not a critical problem given the large diameter of all targets). The slit aperture was set to either

1.0 cm vs. 1.0 cm or 1.5 cm vs. 1.5 cm depending on the beam energy, with never more than 3% of the beam intensity intercepted by the slits. The plastic scintillators S10-S14, behind the BNB, were used to tune the beam on axis.

Additional annular plastic scintillator detectors with different inner/outer diameters, not shown in the scheme (Fig.5), could be set, centered on beam axis and behind the target at the exit of the scattering chamber. These detectors, used as transverse momentum detectors for the inelastically scattered incident particle, revealed a strong correlation between this transverse momentum and the neutron multiplicity in a qualitative way. Although the corresponding data were too crude to be quantitatively exploited from the present experiment, this information could be investigated more thoroughly in future experiments since it provides additional constraints on the physical process generating the neutrons.

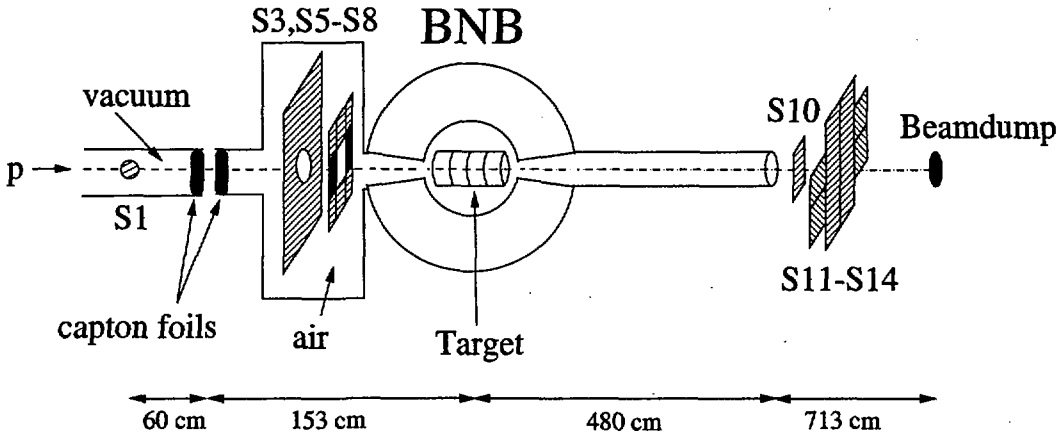

Fig. 5. Scheme of the experimental arrangement (not to scale) showing the Berlin Neutron Ball (BNB) with auxiliary plastic scintillator detectors S_1, S_3, S_{5-8}, S_{10}, S_{11-14} (for details, see text).

As suggested in the scheme of Fig.5, most of the experiment has been run with the target in the air, the beam pipe being closed by a thin capton foil (located about 60 cm downstream from S1). For thick targets it was checked that the extra material (thin capton foil + air) did not impair the quality of the data. Nevertheless, a first-order correction was performed by subtracting the neutron production in absence of target. For thin targets (less than about 1 cm thick), the measurements were performed with the target in vacuum in order to minimize the spurious reactions.

The BNB exit pipe was conical (not centered on the target point), defining an opening of ± 9.7 degrees and ± 5.3 degrees for the inner and outer parts, respectively. This limited angle led to only a small loss of solid angle for the BNB but had some drawbacks in the present measurements. Indeed, due

to multiple scattering, some of the incident particles were scattered into the forward active part of the BNB, generating a prompt signal. These events could easily be confused with other events resulting from a weak nuclear inelastic scattering, with the scattered proton entering the active part of the BNB and delivering also a prompt signal of large amplitude. In the next section, it will be explained how these different types of events were unraveled.

Another and more general question is related to the spurious neutron production from the interactions of the particles escaping the target (high-energy particles from the intra-nuclear cascades) and penetrating the liquid scintillator tank. These neutrons were not experimentally distinguishable from those generated within the target and their contribution could only be estimated from model calculations. An estimate using the LAHET[20] code led to an average of 1 and 2.5 neutrons for a 1.2 and 2.5 GeV incident protons respectively for thin targets. However for the thickest targets, when the inter-nuclear cascades can fully develop, and thus the initial energy is shared among many secondary particles, the latter have low energy (as shown by the reduced light yield in the prompt signal). Therefore the contribution of spurious neutrons became then negligible.

2.4 Master triggers

Two ways of triggering were applied. The master trigger was either given simply by the presence of an incident particle seen by S1 (for targets thicker than 5 cm), or with the additional requirement of a prompt signal greater than 2 MeVee from the BNB (for thinner targets). For thick targets the beam intensity ranged typically from 200 protons per second (pps) for the 35 cm-thick targets up to 1000 pps for the 5 cm-thick targets and several thousands or tens of thousands of pps for even thinner targets. For the thick targets, due to the large reaction probability, a condition on the occurrence of a nuclear reaction was not needed and the acquisition system not overloaded with uninteresting data. This was obviously not possible in thin target measurements with a much more intense beam. The requirement of a nuclear reaction provided by the presence of a prompt-light signal was thus imposed in the master trigger. Under both triggering conditions, the prompt analog signal was recorded, thus making it possible to determine off-line the reaction probability, P_{reac}, whatever the target thickness. It has been checked for targets thinner than about 5 cm and at all bombarding energies that the way of triggering did not affect the pattern of the neutron multiplicity distributions. In contrast, for thicker targets, especially at low bombarding energy, a loss of events with rather low neutron multiplicity is evidenced in the exclusive data (Fig.6). For these events which correspond to a rather weakly inelastic and single interaction in the target, the leading high-energy particle escapes through the forward hole of the

BNB and the generated light arises mostly from neutrons and gamma-rays. The neutrons, mostly of evaporation origin, generate the prompt light with a large quenching factor and the γ-rays are strongly absorbed in the massive target. As a result, the prompt signals are weak for such events and some of them do not overcome the electronic threshold of 2 MeVee, leading to a loss of events.

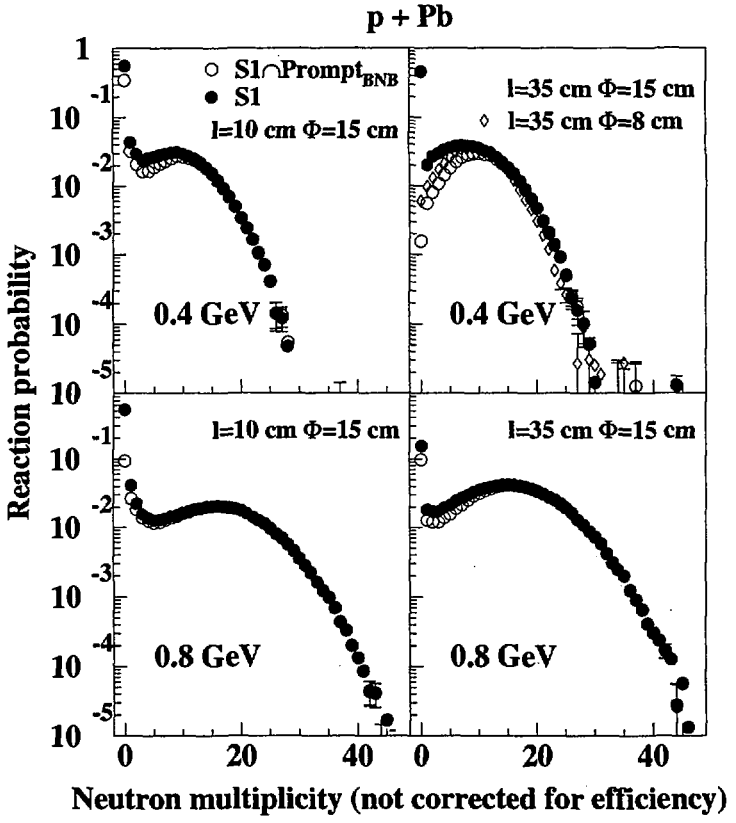

Fig. 6. Neutron multiplicity distributions (not corrected for detector efficiency) as recorded with the inclusive (filled symbols) and exclusive (open symbols) trigger conditions for 0.4 GeV (upper panels) and 0.8 GeV protons (lower panels), as a function of the Pb target size. All dots refer to 15 cm-diameter targets and the diamond to the 8 cm-diameter target.

In conclusion, the trigger conditions which have been adopted for the data taking were carefully checked in order to ensure the minimum bias for both the neutron data and the reaction probability data. For bombarding energies of 1.2 GeV and above, it was checked on the thickest targets that the requirement of the prompt light signal does not corrupt appreciably the observation of events at low neutron multiplicity and the occurence of a nuclear reaction has thus been established by the presence of a prompt light signal. In contrast, at the lower two bombarding energies, the presence of the light signal was

not required but solely the detection of at least one neutron was used for this purpose. The detection of a single neutron is still meaningful because of the very low background ($\simeq 0.1$). It must be noted that when using this procedure for numbering the reaction events, the zero-neutron reactions are not counted. The reaction probability is thus slightly underestimated but much less than in the case where a prompt light signal is required (see Fig.6).

3 DATA ANALYSIS

For each registered event, the neutron multiplicity was read out from a scaler counting the delayed neutron captures on Gd.

Although the off-center incident particles were largely rejected with a high efficiency using the S3, S5-S8 veto detectors, some particles scattered either by the S1 detector or by the capton foil or the air could touch either the BNB entrance or exit pipe, thus inducing parasitic nuclear reactions. These events could be easily rejected by applying a restrictive condition on the time of flight between S1 and the BNB. Moreover the background generated by all extra materials (S1, foil, air) encountered by the beam was measured in absence of target and subtracted from the data obtained in presence of target. This subtraction has been performed after both distributions have been unfolded for correlated background.

Other corrections had to be performed when investigating the reaction probabilities. Even though the general pattern of the light yield versus neutron multiplicity and target thickness is fairly well understood as already indicated in sect. 2.2, some features deserve more attention. For instance, the light spectra exhibit on top of a rather smooth distribution, a spike associated with rather low neutron multiplicities (Fig.7). The spike intensity increases with decreasing bombarding energy and also with target thickness before decreasing for the thickest targets. Moreover the associated light yield decreases with increasing bombarding energy. The corresponding events are identified as the result of multiple scattering of the incident protons in the target, followed by their interaction with the scintillator in which they lose part of their energy. There, they may create only a few neutrons considering the low mass of the elements from which the scintillator is essentially made. The energy loss -as observed as a light yield in BNB- follows quite closely the expectations for a proton projectile crossing 50 cm of liquid scintillor for different initial energies. The effect is maximal for medium-thick targets with e.g. thicknesses increasing from 17 cm at 1.2 GeV up to 30 cm at 2.5 GeV for a Pb target. On one hand, a minimum thickness is indeed needed to scatter the proton to a sufficiently large angle where it intercepts the scintillator tank. On the other hand, when increasing further the target thickness, nuclear reactions become

more and more probable and these spurious events then tend to disappear.

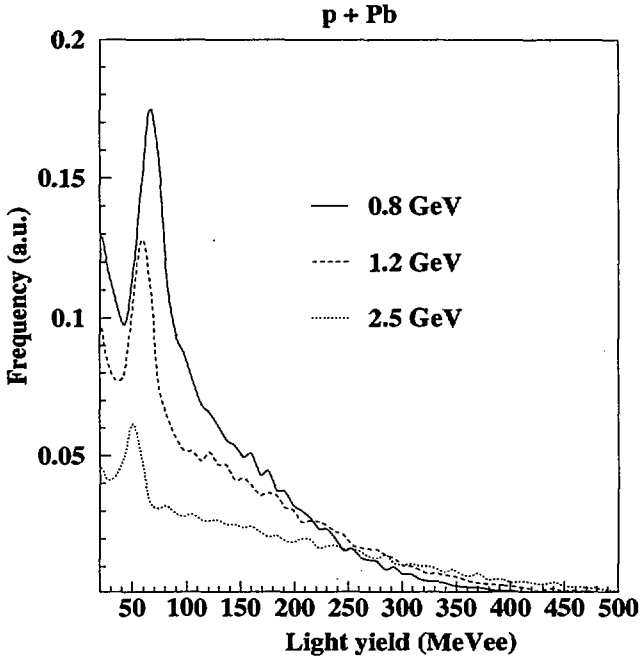

Fig. 7. Light yields for 0.8, 1.2 and 2.5 GeV p induced reactions on a 2 cm thick Pb target and gated with a neutron multiplicity lower than 5. The spikes on top of the smooth spectra were readily visible as a separated island in the two-dimensional pictures of Fig.4 for low neutron multiplicity events.

These multiple scattering events of electronic origin should not be interpreted as nuclear reactions. Being not able to distinguish these events on experimental grounds from those resulting from a weakly inelastic reactions (with the leading particle being scattered into the BNB tank), a simulation has been performed in order to assess the fraction of the former events. For this purpose a reasonable beam profile with a gaussian spatial distribution (σ=2 mm) has been assumed, constrained by the counting rates provided by the veto detectors S5-S8. The multiple scattering has been computed at 1.2 GeV and 2.5 GeV for which additional experimental data were obtained with a medium-thick target placed at different distances with respect to the center of the BNB. These data have helped to constrain the angular aperture of the incident beam. The multiple scattering has been computed using the formulation of Lynch and Dahl [21] as a function of the decreasing energy of the beam propagating through the target. The corrections thus performed on the reaction probability amount to at most 10 % (for a Pb target from 15 to 20 cm, thick) and 2.0 % (for the 35 cm thick Pb target) for 1.2 GeV and 2.5 GeV, respectively. A similar effect is expected at the intermediate energy of 1.8 GeV, although the lack of experimental data with two positions of the target within the tank has not allowed to check it in a quantitative way. The

effect at 1.8 GeV has thus been interpolated between the 1.2 and 2.5 GeV results. The same effect could not be quantified at 0.4 and 0.8 GeV where the multiple scattering is expected to be even more important for thinner targets. However, the 400 and 800 MeV beams being stopped within 14 and 40 cm of Pb, respectively, it can be considered that at least the 35 cm data (for instance) are not or only very weakly affected.

In conclusion, the occurrence of spurious events has been taken into account and corrected whenever possible. It must be stressed that when evaluating the number of neutrons emitted per incident proton -the quantity of interest for the neutron source designers- the spurious events do not bias the results in so far as the number of neutrons generated in such events is fairly low.

4 EXPERIMENTAL DATA

In this section, the data relative to the reaction probabilities, interaction lengths and cross sections will be presented first, and the data relative to the neutron production will be shown afterwards.

4.1 The reaction cross sections and interaction lengths

As mentioned before, the corrections related to spurious reactions in the scintillator due to multiple scattering could be estimated at 1.2 and 2.5 GeV. The survival probability of the incident particle (1-P_{reac}), where P_{reac} is the reaction probability, is shown in Fig.8 for the Pb, Hg and W targets at both energies. A constant logarithmic slope of the survival probability for all three targets at 2.5 GeV bombarding energy indicates a constant reaction cross section, independent of the remaining proton energy when the proton gets deeper inside the target. Such a property is well known for proton-nucleus reactions above 100-200 MeV[22]. The constant logarithmic slope is also observed at 1.2 GeV for the Pb target but no longer for the thick Hg and W targets with a diameter of 15 cm. Such an effect is related to the strong absorption, within the target, of the particles which would have generated the light in the BNB. Indeed, and as shown in Fig. 8, by reducing the diameter of the W target from 15 down to 8 cm, the linearity of the slope is essentially recovered. As demonstrated in Fig. 9, a large amount of light is absorbed when increasing the diameter of the W target. When the light yields become similar for the W (8 cm-in-diameter) and Pb (15 cm-in-diameter) targets, the proton survival probability behaves as expected. A similar absorption effect is likely at 1.2 GeV for the Hg target, although attenuated as compared to what is observed for W due to its lower density.

In addition to enhancing the neutron production, as shown in Fig.9 and as it will be discussed in detail later on, increasing the target diameter has also a shielding effect against parasitic radiations hitting the elements surrounding the target in a genuine spallation assembly for neutron production. The present experimental setup was optimized for the neutron detection but not well suited for investigating the characteristics of the other leaking particles (nature, abundance and angular distributions of charged, neutral particles and γ-rays); their contribution to the measured light cannot be unfolded. Specific measurements of the characteristics of all emitted particles would be of great interest[23] for bringing additional observables and thus more constraints to the models and obviously for the target designers of spallation plants.

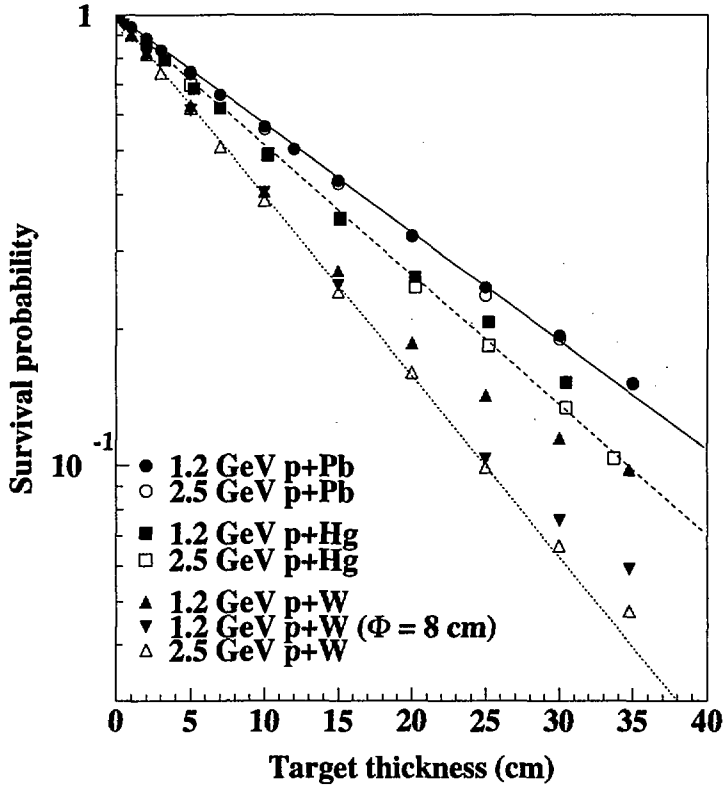

Fig. 8. Survival probability of the incident particle as a function of target thickness for 1.2 and 2.5 GeV on Pb, Hg and W target. For each target, the straight line (solid, dashed and dotted for Pb, Hg and W respectively) gives the best fit as obtained from the 2.5 GeV data. The uncertainties are typically included within the symbol sizes. All data are for $\phi = 15$ cm, except the specified one.

The survival probability can be written: $1\text{-}P_{reac} = \exp(-L/L_{int})$, where L and L_{int} stand for the target thickness and the interaction lengths, respectively, and P_{reac} for the reaction probability. The interaction lengths, L_{int}, as deduced

from the slopes of the 2.5 GeV data (lines in Fig.8) as well as the deduced reaction cross section σ_{reac}, are given in Table 3, together with the reaction cross sections, σ_{thin}, as obtained in measurements at 0.8, 1.2, 1.8 and 2.5 GeV with thin targets (a few g/cm^2). The data are given with two inelasticity thresholds of 2 and 8 MeVee, expressed in terms of the light yield collected in the prompt signal from the BNB. There is good overall agreement between the cross sections as given by the thick and thin target measurements, although the latter are systematically lower by 4% with the 8 MeVee threshold. In a previous measurement on Pb at 1.2 GeV[9], the cross section deduced from the interaction length was found to be 1.65 b in good agreement with the value obtained in the present experiment. It must also be noted that the cross sections as deduced from the thin target measurement in ref.[9] and in the present work are in perfect agreement. The effect of the inelasticity threshold on reaction cross sections is quite visible in Table 3 with data obtained for the 2 and 8 MeVee thresholds. Being able to set the threshold as low as 2 MeVee,

	2 MeVee threshold			
	L_{int}	σ_{reac}	σ_{thin}	σ_{HERMES}
Pb	18.00±0.3 cm	1.69±0.03 b	1.71±0.14 b	1.73 b
Hg	15.06±0.4	1.64±0.05	1.57±0.26	1.71
W	10.84±0.2	1.46±0.03	1.49±0.17	1.62
	8 MeVee threshold			
	L_{int}	σ_{reac}	σ_{thin}	
Pb	18.38±0.3 cm	1.65±0.03 b	1.58±0.03 b	
Hg	15.39±0.3	1.60±0.03	1.44±0.13	
W	11.18±0.2	1.41±0.03	1.35±0.07	

Table 3
Interaction lengths, L_{int}, and cross sections as deduced from the survival probabilities, σ_{reac} (Fig.8) and from direct thin target measurements, σ_{thin}, as given for 2 detection thresholds on the prompt light (for details see text). Also are listed the reaction cross sections used in HERMES.

the present data are probably as reliable as those obtained by the standard attenuation method[24] which also suffers from inelasticity threshold effects. There is a good agreement between the cross sections presently measured with an inelasticity threshold of about 2 MeV and those extracted from other studies[22]. The reaction cross sections increase roughly as the two third power of the target mass, as expected. All this demonstrates that the BNB response

is well under control and that this instrument is fully adapted for measuring the total spallation reaction cross sections.

For the Hg target, the experimental situation has been made more difficult to control because for the medium- and large thicknesses, the targets are made by a stack of closely packed containers and several steel layers -1 mm thick- thus lay in sandwich within the Hg assembly. The measured data are affected by the presence of the steel containers, whose effect cannot be simply subtracted as for thin targets, since they contribute in both the intra- and inter-nuclear cascades together with the Hg target in an intricate way. In order to appreciate this effect, an assembly of successive Pb (35cm of total thickness) and Fe targets similar to the one used for the Hg target and containers has been bombarded at 1.2 GeV and the data compared with those obtained for a pure Pb target, 35 cm thick. A decrease of 0.4 % in the average neutron multiplicity has been observed with the mixed target.

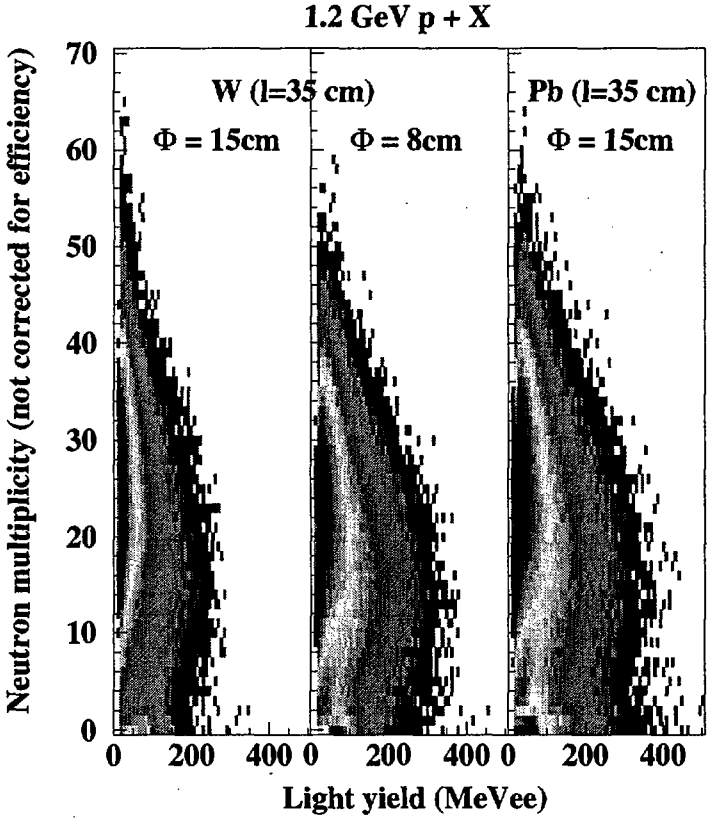

Fig. 9. Distribution of events as a function of light yield and neutron multiplicity (as measured) for different target materials and diameters (all targets are 35 cm thick) and a 1.2 GeV proton beam.

For the thin Hg targets and due to some thickness inhomogeneity of the cells

containing the Hg liquid, we have a systematic difference between σ_{reac} and σ_{thin}, notably larger than for the other materials.

4.2 The neutron multiplicity distributions

The genuine originality of the present experiment and recently performed ones[9][10][11] when compared to much of the previous ones[7] lies in the possibility of extracting neutron multiplicity distributions and not only their average values. This information has, among others, much relevance in the design of accelerator driven subcritical systems[25]. For illustration, Fig.10 exhibits such distributions for 0.8, 1.2, 2.5 GeV protons impinging on thin Pb, Hg and W targets. They have been corrected for uncorrelated and correlated backgrounds. Furthermore for the Hg target, subtraction of the spurious events due to the container has been performed. The distributions look all alike with a bell-shape distribution as a dominant component and an additional weak component at very low neutron multiplicity which arises from weakly inelastic peripheral collisions. The mean neutron multiplicity increases with energy as also shown by Ledoux et al.[26] indicating a larger energy deposition within the nucleus for the more energetic projectile. The data for Pb and Hg, two very close nuclei in the nuclide chart, look very much alike, whereas W, somewhat lighter, exhibits a slightly reduced neutron production. This target effect is consistent with what has been obtained by Enke et al.[19] and Pienkowski et al.[9] over a broader range of nuclei.

For target thicknesses less than 2 mm at most, a single nuclear reaction takes place within the target and the neutron multiplicity distribution results from the intra-nuclear cascade alone (both direct emission and evaporation). When the target gets thicker, the gain in neutron production per incident particle stems from two main origins as shown in Fig.11 and 12. First, the larger thickness allows a primary nuclear reaction to take place with a much larger probability which is by far the most important factor to gain neutrons per incident proton, as is obvious from the gain in the ordinate values dP_{reac}/dN in Fig.11 for increasing target thickness. In addition there is an amplifying effect with the high-energy particles originating from the intra-nuclear cascade able to generate neutrons in secondary (or inter-nuclear cascade) reactions. This latter effect can be estimated by comparing the mean neutron multiplicity per nuclear reaction as a function of the target thickness (Fig.11). The higher the beam energy, the stronger the amplification. At 2.5 GeV on Pb, the amplifying factor is roughly equal to 2 for the target sizes employed.

For a practical purpose, the reaction probabilities as given as a function of neutron multiplicity for a given beam energy and target thickness as they were measured -i.e. without efficiency correction depending on the neutron energy

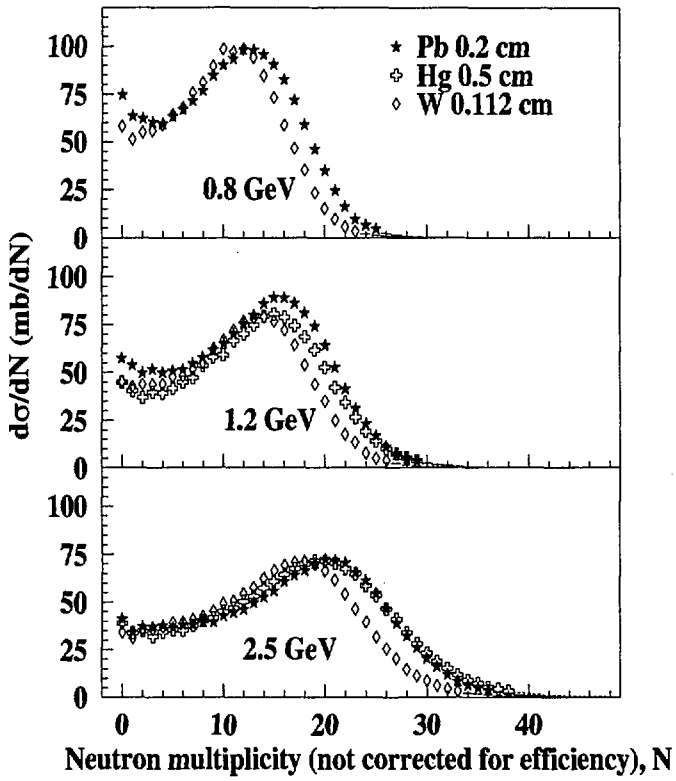

Fig. 10. Differential cross sections ($d\sigma/dN$ given in mb) as a function of neutron multiplicity as measured on thin targets (the data are corrected for background and dead time but not for neutron detection efficiency). Statistical error bars are smaller than symbol sizes.

spectrum- but fully corrected for all other effects (correlated and uncorrelated backgrounds, acquisition and pile-up dead times) have been fitted by means of the sum of an exponential component at low multiplicity and a Gaussian component for the bell-shape component. The following equation (1) has been employed as already done in ref.[10]:

$$\frac{dP_{reac}}{dN} = \frac{S_E}{T_n} \exp(\frac{-M_n}{T_n}) + \frac{S_G}{s\sqrt{2\pi}} \exp(-\frac{(M_n - M_n^{max})^2}{2s^2}) \qquad (1)$$

Such fitted data are easily usable for sake of comparison with any model calculation provided the results of the latter are properly folded with the BNB detection efficiency which is energy dependent, as given in Fig.2. As shown in Fig.11, the data corresponding to the zero neutron channel have not been considered in the fitting procedure. Indeed, these data corresponding to weakly inelastic reactions (below the one-neutron evaporation threshold) and then close to the detection threshold suffer the largest uncertainties. The parameters obtained from the fits with Eq.(1) are listed in Table 4 for the three

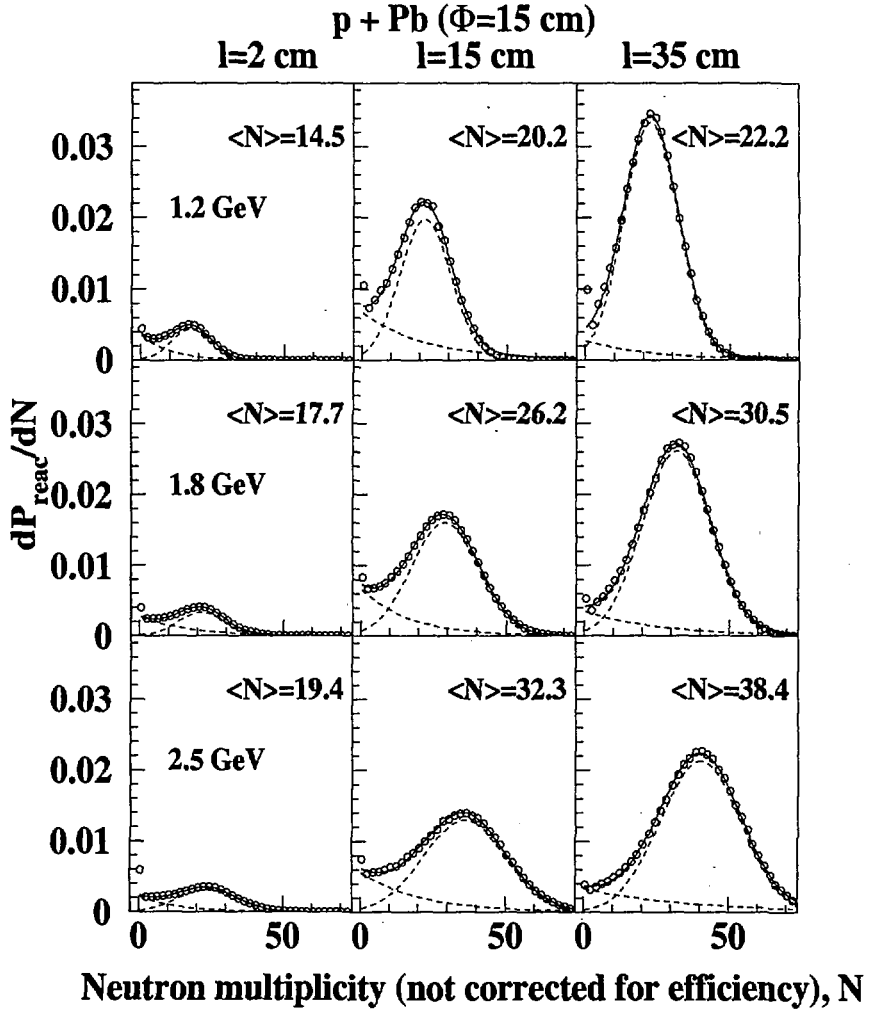

Fig. 11. Reaction probability as a function of neutron multiplicity (the data are corrected for background and dead time but not for neutron detection efficiency) for three bombarding energies. The data are fitted using an exponential plus a gaussian component (dashed lines) and their sum (solid line). The data from the fits are gathered in Table 4. All targets are 15 cm in diameter, the thickness being defined on top of the panels. The mean value ($< N >$) of the distribution is given in each panel. For details, see text.

target materials, the three highest energies and the different target sizes.

The statistical uncertainties, in general, are completely negligible (they lie within the symbol sizes) as can be seen from the small scattering of the data points in all the figures of this paper. The systematic errors due to background correction are also negligible due to the precisely measured multiplicity distributions of correlated and uncorrelated backgrounds with average values of 0.4 and 0.6, respectively. Most of the uncertainty arises from the subtraction of

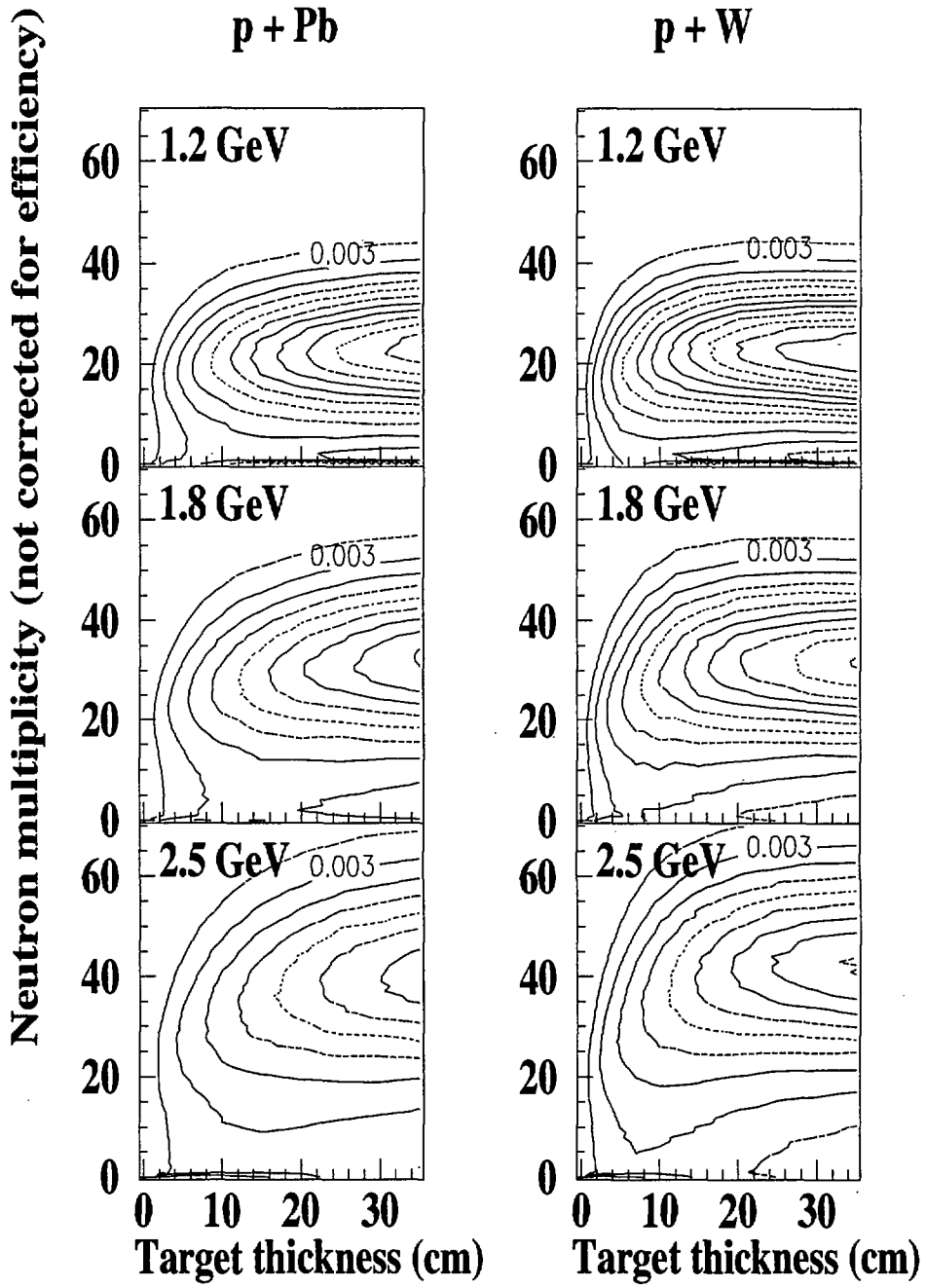

Fig. 12. Two-dimensional display of neutron multiplicity versus target thickness for Pb and W targets and 3 proton energies. The contours represent the reaction probability (successive lines separated by 3.10^{-3}). All targets are 15 cm in diameter.

the estimated neutrons produced within the scintillator after multiple scattering of the projectile in the target. It affects only the low multiplicity channels (up to 5 neutrons) and introduces there an uncertainty of about ±20%.

A synthetic picture of the neutron multiplicity distributions is given in Fig.12 for the Pb and W targets of 15 cm in diameter, as a function of the different measured target thicknesses for three bombarding energies. It illustrates in great detail the influence of the different entrance channel parameters and exshibits the wealth of information gathered in the present experiment, as listed in Table 4.

4.3 General comments on the neutron production as a function of entrance channel parameters

The mean neutron production multiplicity, corrected for the corresponding detection efficiency as given in Fig.3, is presented as a function of the beam

energy, the target material and the target thickness either associated with a nuclear interaction (exclusive data) in Fig.13 or normalized to the number of incident particles (inclusive data), in Fig.14. At 0.4 and 0.8 GeV corrections of multiple scattering could not be performed due to a lack of experimental information. Therefore only those data points corresponding to stopped beams for which such a bias does not exist are displayed in Fig.13. In contrast, in Fig.14, all data points have been included since the contribution of the spurious events remains negligible when normalized to the number of incident protons.

With thin targets i.e. when probing a single reaction per event (no inter-nuclear cascade), it is shown in Fig.13 that the average neutron multiplicity does not increase linearly with incident proton energy. This is due to two reasons: first the heating of the nuclei does not increase proportionally to the incident energy and, second, the more a heavy nucleus is heated the more the competition of evaporated charged particles with neutrons becomes important.

The increase in projectile energy has mostly a positive impact on neutron production in thick targets in so far as it permits inter-nuclear cascades to develop more efficiently. Considering for instance the W targets, the multiplication factor is 1.55 at 1.2 GeV and 2.14 at 2.5 GeV when increasing the target thickness from 1 to 35 cm, as shown in Fig.13.

The experimental data have been compared with the results of the HERMES code[18], run with the same set of input parameters for all targets and energies: the level density parameter $a = \frac{A}{8}(1 + 1.5\frac{(A-2Z)^2}{A^2})$ is used and fission is allowed in the calculations. The overall agreement is satisfactory. However, as pointed out by Enke et al.[19] the HETC-type simulation codes, either in

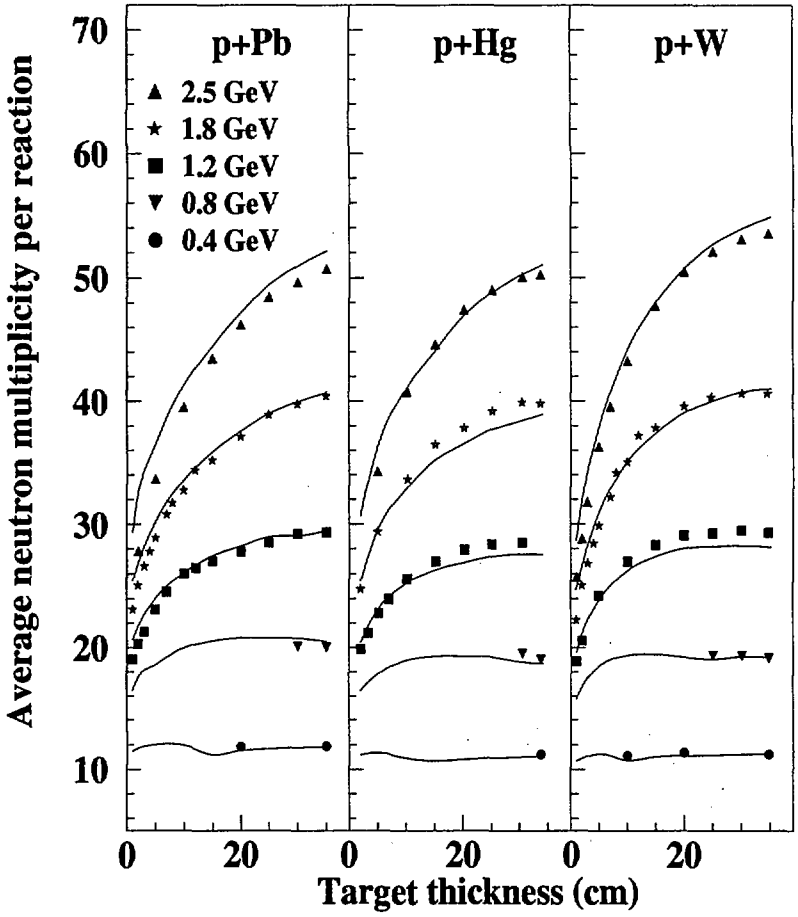

Fig. 13. Average neutron multiplicity per nuclear reaction as a function of target thickness and beam energy for the Pb, Hg and W materials. The experimental data are fully corrected (background and detection efficiency). All targets are 15 cm in diameter. Statistical error bars are within the symbol sizes. The solid lines result from a HERMES calculation. For details see text.

LAHET[20] or in HERMES[18] and applied for thin targets strongly overestimate the excitation energy reached by the nucleus and thus the multiplicity of evaporated particles. The effect was readily visible on evaporated charged-particles[19] but appears to be more difficult to discern on neutrons due their comparatively larger multiplicity. For the thickest targets the good agreement between experimental data and modeled data must somewhat result from a compensation effect. Indeed the excess of energy brought in the first heated nucleus when using HETC-type codes is no longer available in the inter-nuclear cascade induced by secondary reactions.

The saturation regime is nearly reached for the neutron production with a 30 cm thick W target at 800 MeV, while this is no longer true at higher energies as shown by both experimental data and simulations (Fig.13 and 14-top). In order to be reached, the saturation regime requires even thicker targets for less dense materials such as Pb and Hg.

As for the nature of the material, if W appears to be more neutron prolific than Pb or Hg for the same quantity of material expressed in cm of material (Fig.13 and 14-top), the reverse is true when the thickness is expressed as a function of the number of atoms per unit area of the target although the difference is weak with the Hg and Pb data (Fig.14-bottom). This means that, in this domain of target Z (from Z = 74 up to Z = 82), there is a rather low sensitivity of the neutron production to the target Z (as also seen in Fig. 10).

Such is not the case in the region of higher Z materials as was observed in ref. [9][10]: a U target is more prolific - by about 50% - than a Pb target because of the many neutrons generated through several fission reactions occurring on the average per incident particle. In contrast, for W, Hg and Pb which are all poorly fissile materials (and even poorer are the species produced at the end of the INC cascade) the contribution of fission neutrons is negligible.

Under given conditions of beam energy it is important to stress that W provides a more compact source than a less dense material for a similar neutron intensity of the spallation source, resulting in a larger neutron flux. The difference considering Hg and Pb is much attenuated taking into account the weaker difference of density of the these two materials ($\varrho_{Hg}/\varrho_{Pb}$= 1.19 as compared to ϱ_W/ϱ_{Pb}= 1.70).

The influence of the target diameter on the neutron production is shown in Fig.15 as a function of the target thickness and the bombarding energy for W. For the thickest targets at high energy, one would obviously gain in increasing further the target diameter as intuitively expected. The HERMES simulation

reproduces the overall experimental data satisfactorily however it has a tendency to overestimate the neutron production for the small diameter targets (ϕ = 8cm) at 2.5 GeV.

The most interesting quantity for neutron source designers is the number of neutrons generated per incident particle, as shown in Fig.14-top for given characteristics of the target. The almost linear rise of all curves with increasing target thickness for rather thin targets denotes nothing but an increase of reaction probability. As explained before, the effect of neutron multiplication in secondary collisions is then very modest. In contrast, with targets of thickness corresponding to 3 reaction lengths i.e. about 30 cm for W, when 95% of the incident particles have undergone reaction, the neutron gain with

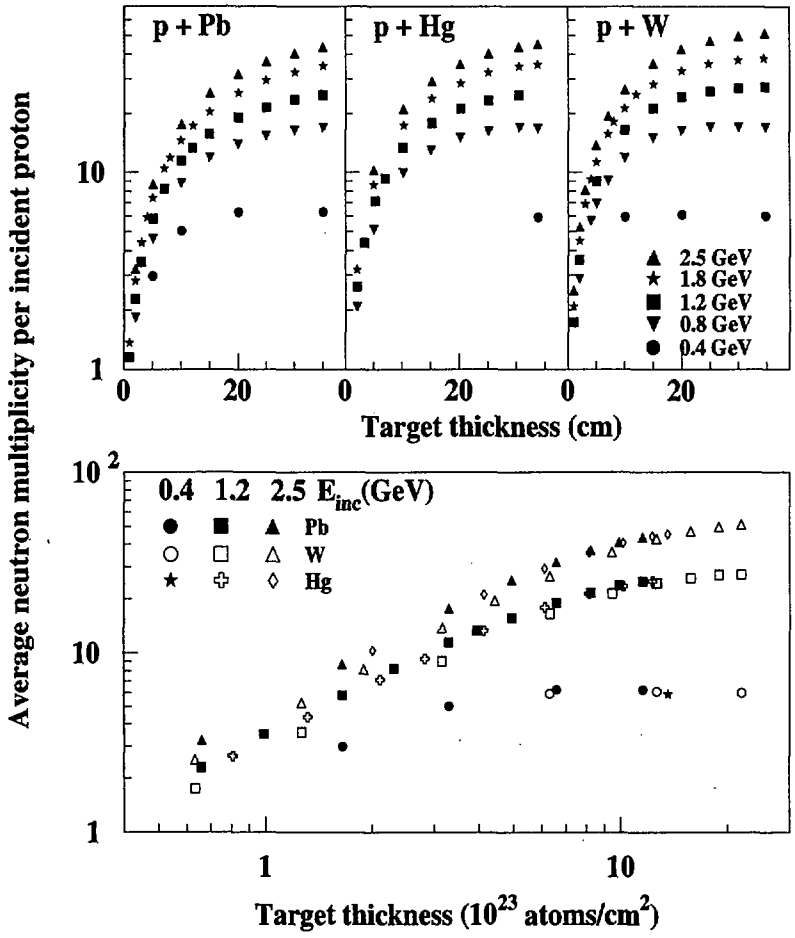

Fig. 14. Top : Average neutron multiplicity per incident proton as a function of target thickness (given in cm) and beam energy for the Pb, Hg and W materials. The experimental data are fully corrected (background and detection efficiency). All targets are 15 cm in diameter. Bottom : same results as above but the thickness is given in units of $10^{23} atoms/cm^2$.

increasing thickness is strongly dominated by secondary reactions. This is best seen for the highest energies considered in this experiment. There the saturation is not reached in the neutron production and increasing the target size both in thickness and diameter would then be favorable. In contrast, at the lowest energies no gain is expected from a voluminous target: the projectiles are electronically stopped before reaching several interaction lengths and the secondary light particles have low energies, with the charged ones being even more sensitive to the electronic stopping power.

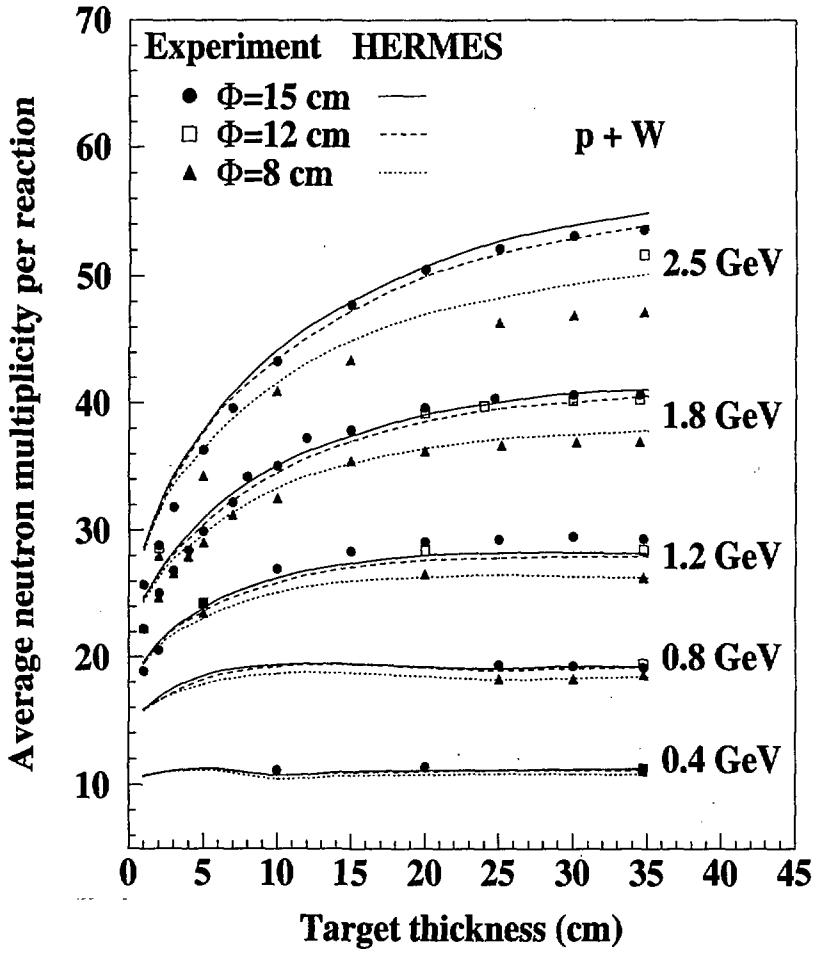

Fig. 15. Average neutron multiplicity per nuclear reaction as a function of target thickness and energy for a 15 cm (filled circle), 12 cm (open square) and 8 cm (filled triangle) in diameter W target. The experimental data are fully corrected (background and detection efficiency).

4.4 The neutron economy

The running cost of the proton accelerator is an important parameter when designing a neutron spallation source. Another interesting quantity is the neutron cost, shown in Fig.16, as the number of produced neutrons normalized to the unit beam energy per incident particle. The Pb target has been chosen because of the number of existing data, all data being obtained in the same experimental approach[10][11]. The previously published data are corrected for detection efficiency in the same way as the present data. Doing so there is an overall good agreement between old and new data. At most a 7% discrep-

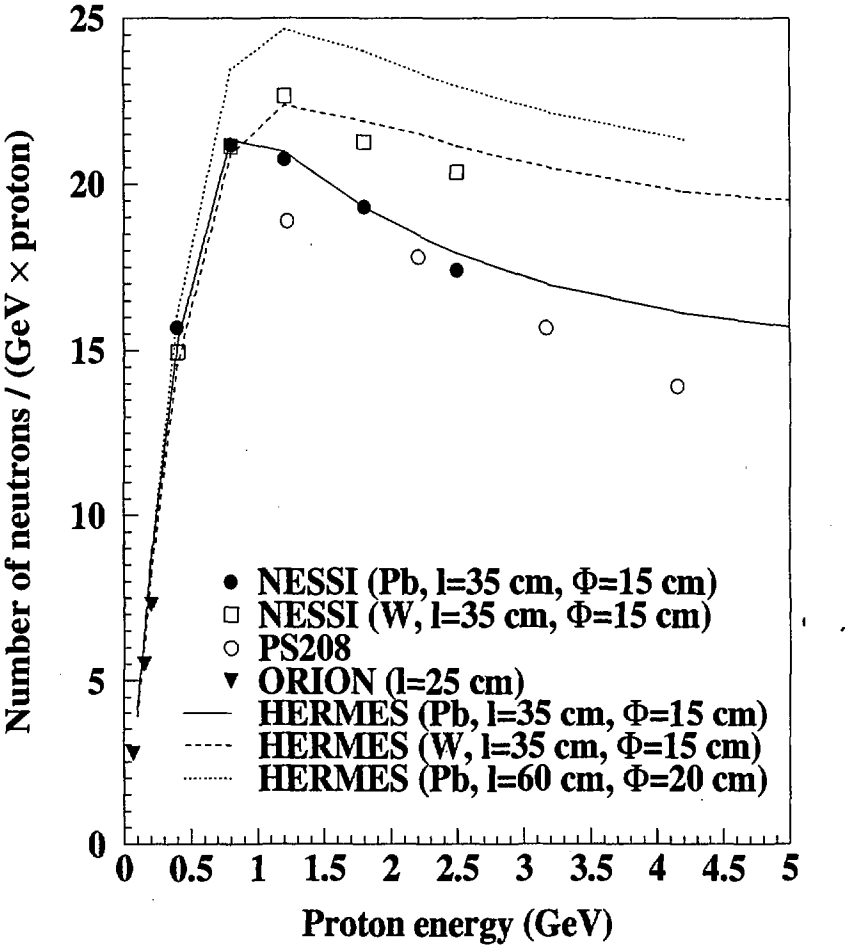

Fig. 16. Average neutron multiplicity (fully corrected) per unit energy (expressed in GeV) and per incident proton as a function of beam energy. Previously published data at high (PS208 [9]) and low energy (ORION [11]), respectively, have been added up to the present (NESSI) data. Statistical errors are within the symbol sizes. The solid, dashed and dotted curves are the results of HERMES simulations for Pb : 35*15 cm, Pb : 60*20 cm and W : 35*15 cm targets, respectively.

ancy is observed at 1.2 GeV which might be related to a different quality of the employed beams and target purities.

A maximum in the neutron number is observed for Pb at 0.8-1.0 GeV, defining the optimum conditions, as far as the economy is considered. The abrupt, low energy part of the curve reflects once more the influence of the electronic stopping which is a strong but unavoidable phenomenon hampering neutron production at low energy while the slow descent above 1.0 GeV might be related to the target size. Indeed, when considering the curves of Fig.14-top, it

is shown that the saturation in the neutron production is essentially obtained for the thickest targets at the two lowest incident energies at best but not for the three highest ones. Clearly for the latter energies, thicker targets would have provided more neutrons and so far the maximum observed between 0.8 GeV and 1.0 GeV in the neutron "economy" cannot be considered as fully meaningful. Model calculations predict substantial gains in neutron production at the highest energies when increasing the target thickness from 35 to 60 cm and the diameter from 15 to 20 cm (solid and dashed lines in Fig.16 for the smallest and biggest targets, respectively). It is seen that the threshold energy for the maximum production is somewhat shifted and that the descent suggested at high energy in Fig.16 is somewhat less steep for massive targets. Clearly, more experimental data would be needed in order to confirm these trends. However, without these data and taking into account the difference of density between Pb and W, we can already consider the data from the 35 cm-thick and 15 cm-in-diameter W target. Clearly the gain in production, when compared with the same sized Pb target, is substantial with the expected leveling at high energy suggested by both the data and simulations (dotted line). This would justify further experimental investigations with more and more massive targets with increasing energy and also with energies beyond 2.5 GeV. In a very recent experiment at KEK[27], 194.7 neutrons have been measured on average for a 12 GeV proton impinging on a Pb cylinder, 20 cm in diameter and 60 cm in length.

Gaining a better knowledge on the neutron economy may have important consequences on the design of a high-intensity neutron facility. Indeed, if we assume that the neutron economy remains rather stable over a broad range of incident energies, then, for a given neutron production the beam intensity could be reduced if higher energies are employed. As a consequence the load on the window separating accelerator and target could be reduced accordingly, noting that the electronic energy loss in the window remains essentially constant above 1.5 GeV while, at the same time, the major cause for radiation damage, He production, increases less than linearly with proton energy[19]. Since the window design appears to be one of the hardest problems to be solved for the spallation neutron source, in somewhat direct connection with the neutron economy, further investigations need to be performed above 1 GeV with the exploration of thicker targets.

It should also be stressed that there are quite different requirements for neutron production for a pulsed source used for neutron scattering and a steady production for feeding a hybrid reactor:

-In the first case, one needs high neutron fluxes passing through the target close to which the moderators have to be positioned. Thus additional neutrons produced from a massive target would be of no use.

-In contrast, for transmutation or accelerator driven reactors, all neutrons produced in a big target are of interest in evaluating the neutron economy of such systems.

5 SUMMARY

New experimental data have been gathered for neutron production by spallation of proton beams at 0.4, 0.8, 1.2, 1.8 and 2.5 GeV on a series of W, Hg and Pb targets of different sizes. Making use of a high efficiency 4π-Gd loaded, liquid scintillator, neutron-detector (BNB) sensitive to all types of particles (neutrons, charged particles, gamma-rays) allows direct information on reaction probabilities and the full neutron multiplicity distributions to be obtained. In thin targets where there is a single nuclear reaction (i.e. no inter-nuclear cascade), the neutron production is shown to depend rather weakly on both target material (for $74 \leq Z \leq 82$) and beam energy. This is understandable considering the characteristics of the intra-nuclear cascade process and the well known decay properties of hot heavy nuclei. In a single p-nucleus collision, only a rather small fraction of the incident energy (25-30 % at most, and much less on the average) can be found as excitation energy in the struck nucleus and at high excitation energy a larger and larger fraction of this energy is removed by charged particles at the expense of neutrons. With increasing target thickness, the gain in neutron production is primarily due to the increase in the reaction probability and to a lesser extent to a better utilization of the primary beam energy through inter-nuclear cascades leading to several excited nuclei and thus several neutron contributions per incident particle. For targets with thicknesses corresponding to several interaction lengths and with beams of sufficient energy to not suffer too much from the electronic losses (i.e. $E > 1$ GeV) the secondary reactions play a crucial role. Above 1 GeV, the present data should be complemented with thicker-target data in order to establish more firmly the details of the neutron economy. This is an important issue since if a bombarding energy of several GeV instead of 1 GeV would lead to a similar neutron production cost, then the load on the target window could be reduced for the same global neutron production by using a lower beam intensity.

Acknowledgements

We are indebted to the COSY staff for the good beam quality. This work was partly supported by the EU-TMR project ERBFMRXCT980244, by the german Srategiefonds project R&D for ESS of the Helmholtz Gesellschaft and

by the french GEDEON project.

References

[1] The European Spallation Source Study, vol. III, The ESS Technical Study, report ESS-96-53-M, 1996, ISBN 0902376659

[2] B.Appleton, Proc. ICANS-XIII, Report PSI 95-02 (1995), p 814-818

[3] S.Nagamiya, JAERI-KEK joint project on high intensity proton accelerator, 9^{th} International Conference on Radiation Shielding Oct. 17-22, 1999, Tsukuba Japan

[4] C.D.Bowman, E.D.Arthur, P.W.Lisowski, G.P.Lawrence, R.J.Jensen, J.L. Anderson, B.Blind, M.Cappiello, J.W.Davidson, T.R.England, L.N.Engel, R.C.Haight, H.G.Hughes III, J.R.Ireland, R.A.Krakowski, R.J.LaBauve, B.C.Letellier, R.T.Perry, G.J.Russel, K.P.Staudhammer, G.Versanis and W.B.Wilson, Nucl. Instr. Meth. A 320 (1992) 336.

[5] C.Rubbia, J.A.Rubio, S.Buono, F.Carminati, N.Fiétier, J.Galvez, C.Gelès, Y.Kadi, R.Klapisch, P.Mandrillon, J.P.Revol and C.H.Roche, Report No. CERN/AT/95-44(ET) (1995)

[6] J.S.Fraser et al., Phys. Can. 21 (1966) 17; and T.W.Armstrong et al., Nucl. Inst. Meth. 222 (1984) 540.

[7] R.G.Vassilkov, V.I.Yurevich, Proceedings ICANS-XI, Tsukuba, (1990) 340.

[8] V.A.Nikolaev, V.I.Yurevich, R.M.Yakovlev and R.G.Vassilkov, Proceedings ICANS-XI, Tsukuba, (1990) 612.

[9] L.Pienkowski, F.Goldenbaum, D.Hilscher, U.Jahnke, J.Galin and B.Lott, Phys. Rev. C 56 (1997) 1909.

[10] D.Hilscher, U.Jahnke, F.Goldenbaum, L.Pienkowski, J.Galin and B.Lott, Nucl. Instr. and Meth. A 414 (1998) 100.

[11] B.Lott, F.Cnigniet, J.Galin, F.Goldenbaum, A.Liénard, A.Péghaire, Y.Périer and X.Qian, Nucl. Instr. and Meth. A 414 (1998) 117

[12] J.Galin and U.Jahnke, J. Phys. G: Nucl. Part. Phys. 20 (1994) 1105

[13] R.Wigmans, Nucl. Instr. and Meth. A 259 (1987) 389

[14] U.Jahnke, G.Ingold, D.Hilscher, H.Orf, E.A.Koop, G.Feige, R.Brandt, Lecture Notes in Physics 179, Springer, Berlin, 1983, p 179

[15] X.Ledoux, F.Borne, A.Boudard, F.Brochard, S.Crespin, D.Drake, J.C. Duchazeaubeneix, D.Durand, J.M.Durand, J.Fréhaut, F.Hanappe, L.Kowalski, C.Lebrun, F.R.Lecolley, J.F.Lecolley, F.Lefebvres, R.Legrain, S. Leray,

M.Louvel, E.Martinez, S.I.Meigo, S.Ménard, G.Milleret, Y.Patin, E.Petibon, F.Plouin, P.Pras, L.Stugge, Y.Terrien, J.Thun, M.Uematsu, C.Varignon, D.M.Whittaland, W.Wlazlo, Phys. Rev. Lett. 82 (1999) 4412

[16] S.Meigo, H.Takada, S.Chiba, T.Nakamoto, K.Ishibashi, N.Matsufuji, K.Maehata, N.Shigyo, Y.Watanabe and M.Numajiri, Nucl. Instr. Meth. A 431 (1999) 521

[17] J.Poitou, C.Signarbieux, Nucl. Instr. Meth. 114 (1974) 113

[18] P.Cloth, D.Filges, R.D.Neef, G.Sterzenbach, Ch.Reul, T.W.Armstrong, B.L.Colborn, B.Anders, H.Brückmann, Report Jülich 2203 (1988)

[19] M.Enke, C.M.Herbach, D.Hilscher, U.Jahnke, O.Schapiro, A.Letourneau, J..Galin, F.Goldenbaum, B.Lott, A.Péghaire, D.Filges, R.D.Neef, K.Nünighoff, N.Paul, H.Schaal, G.Sterzenbach, A.Tietze, L.Pienkowski, Nucl. Phys. A657 (1999) 317

[20] R.E.Prael, H.Lichtenstein, LAHET code system LAHET 2.7d, Los Alamos National Laboratory Report LA-UR-89-3014 (1989)

[21] G.R.Lynch and O.I.Dahl, Nucl. Instr. Meth. B58 (1991) 6

[22] H.P.Wellisch and D.Axen, Phys. Rev. C 54 (1996) 1329

[23] U.Jahnke et al. have proposed such experiments as a follow-up of the present measurements.

[24] J.J.H.Menet, E.E.Gross, J.J.Malanify and A.Zucker, Phys. Rev. C 4 (1971) 1114

[25] I.Parzit and Y.Yamane, Nucl. Instr. Meth. A403 (1998) 431

[26] X.Ledoux, H.G.Bohlen, J.Cugnon, H.Fuchs, J.Galin, B.Gatty, B.Gebauer, D.Guerreau, D.Hilscher, D.Jacquet, U.Jahnke, M.Josset, S.Leray, B.Lott, M.Morjean, B.M.Quednau, G.Röschert, H.Rossner, A.Péghaire, L.Pienkowski, R.H.Siemssen and C.Stéphan, Phys. Rev. C 57 (1998) 2375.

[27] M.Arai, Y.Kiyanagi, N.Watanabe, R.Takagi, H.Shibazaki, N.Numajiri, S.Itoh, T.Otomo, M.Furusaka, Y.Inamura, Y.Ogawa, Y.Suda and S.Satoh, J. Neutron Research 8 (1999) 71.

6 APPENDIX

Table 4
Parameters obtained from the fits of the neutron multiplicity distributions (as measured without efficiency correction) with the relation given by Eq.1. The Mean and the standard deviation, RMS, of these distributions are also given. The mean values once corrected for detection efficiency (Fig.3) lead to the data shown in Fig.13 and Fig.15.

Thickness (cm)	M_n^{max}	s	T_n	$S_G(.10^{-2})$	$S_E(.10^{-2})$	Mean	RMS
Pb - thin targets for respectively 1.2, 1.8, 2.5 GeV							
0.20	15.28	5.25	6.25	0.74	0.32	12.12	7.13
0.20	17.63	5.71	8.25	0.70	0.34	13.35	8.37
0.20	19.95	6.23	10.31	0.67	0.37	13.66	9.95
W - thin targets for respectively 1.2, 1.8, 2.5 GeV							
0.11	13.38	4.97	6.14	0.64	0.24	11.11	6.30
0.11	15.36	5.48	7.54	0.67	0.28	12.12	7.46
0.11	17.34	6.01	8.91	0.69	0.32	12.31	8.86
Hg - thin targets for respectively 1.2, 1.8, 2.5 GeV							
0.50	14.91	5.42	7.30	2.02	0.79	12.33	7.00
0.50	17.67	6.07	8.64	1.93	0.88	13.91	8.42
0.50	19.58	6.93	10.79	2.26	0.99	14.59	9.94
Pb 1.2 GeV $\phi = 8$ cm							
35.00	19.15	8.42	13.53	78.13	7.19	18.40	8.93
Pb 1.2 GeV $\phi = 12$ cm							
35.00	21.08	9.02	14.86	80.32	4.75	20.51	9.43
Pb 1.2 GeV $\phi = 15$ cm							
1.00	16.62	6.21	8.40	3.91	1.94	13.38	8.04
2.00	17.48	6.95	9.28	7.63	3.42	14.45	8.57
3.00	18.31	7.47	10.02	11.24	4.87	15.28	9.06

5.00	19.28	8.34	10.22	18.85	6.05	16.80	9.53
7.00	20.02	8.79	11.57	26.09	7.30	17.96	9.85
10.00	21.10	9.21	11.69	35.45	7.85	19.22	10.18
12.00	21.54	9.31	11.85	40.88	8.33	19.63	10.34
15.00	21.74	9.26	11.65	49.01	7.73	20.15	10.15
20.00	22.11	9.45	12.03	60.24	6.58	20.85	10.20
25.00	22.37	9.40	13.80	68.81	5.78	21.46	10.00
30.00	22.66	9.54	15.59	75.65	4.55	22.05	9.98
35.00	22.70	9.50	15.07	80.37	3.97	22.17	9.86
Pb 1.8 GeV $\phi = 8$ cm							
0.50	18.58	6.59	9.37	1.95	0.87	14.90	8.86
1.00	19.53	7.08	10.86	3.78	1.90	15.72	9.44
5.00	22.85	9.59	12.44	18.83	6.44	19.71	11.24
10.00	24.65	10.51	12.32	35.93	8.23	22.12	11.79
15.00	25.67	10.55	13.15	48.57	9.62	23.38	11.84
20.00	26.21	10.57	14.64	57.48	9.92	24.30	11.76
25.00	26.49	10.55	15.50	65.05	9.76	24.80	11.67
30.00	26.55	10.52	16.88	71.09	9.74	25.14	11.51
35.00	26.51	10.52	17.90	75.82	9.61	25.25	11.45
40.00	26.21	10.71	18.31	81.81	7.34	25.45	11.24
Pb 1.8 GeV $\phi = 12$ cm							
15.00	27.98	11.57	13.94	49.05	8.73	25.77	12.77
20.00	28.77	11.68	13.60	60.35	7.61	27.06	12.66
25.00	29.39	11.45	17.14	66.54	9.16	27.69	12.58
30.00	29.63	11.51	17.19	73.41	7.68	28.30	12.41
35.00	29.73	11.36	19.79	77.18	7.97	28.55	12.25
39.00	29.63	11.36	21.98	80.55	7.38	28.73	12.10
Pb 1.8 GeV $\phi = 15$ cm							

1.00	19.75	7.22	11.85	3.77	1.96	16.04	9.55
2.00	21.07	8.48	12.42	7.65	3.32	17.66	10.43
3.00	22.40	9.19	12.92	11.37	4.85	18.91	11.08
4.00	23.44	9.58	14.42	14.43	6.47	19.92	11.54
5.00	24.22	10.23	13.82	18.38	6.85	20.90	11.93
7.00	25.64	10.97	13.60	25.63	7.98	22.43	12.53
8.00	26.38	11.12	14.30	28.44	8.74	23.21	12.74
10.00	26.98	11.44	13.73	35.02	8.71	24.16	12.83
12.00	28.34	11.62	14.34	39.94	9.62	25.43	13.19
15.00	28.80	11.71	14.48	47.80	9.82	26.20	13.17
20.00	29.99	11.79	14.38	58.67	9.11	27.78	13.13
25.00	31.22	11.87	17.96	64.99	9.91	29.22	13.28
30.00	31.53	11.88	17.64	73.15	8.18	29.98	13.02
35.00	31.68	11.86	19.93	78.44	7.07	30.52	12.71
Pb 2.5 GeV $\phi = 8$ cm							
0.26	20.02	6.72	10.18	0.95	0.40	15.36	9.73
2.00	23.29	9.57	13.11	7.83	3.03	18.97	11.91
10.00	29.53	12.32	15.70	34.69	9.51	25.92	14.29
20.00	32.00	12.54	18.64	56.58	10.98	29.38	14.28
35.00	32.93	12.40	25.20	74.44	11.17	31.33	13.71
Pb 2.5 GeV $\phi = 12$ cm							
35.00	37.28	13.69	20.89	79.55	7.12	35.81	14.82
Pb 2.5 GeV $\phi = 15$ cm							
2.00	23.88	9.98	13.24	7.83	3.08	19.38	12.31
5.00	27.96	12.57	13.96	19.49	5.63	24.16	14.23
10.00	32.76	13.97	15.30	35.25	8.56	29.03	15.77
15.00	35.83	14.18	18.36	46.94	10.53	32.32	16.26
20.00	37.86	14.17	22.44	55.53	12.28	34.63	16.34

25.00	38.93	14.21	23.70	65.81	10.84	36.47	15.99
30.00	39.65	14.23	23.39	71.78	9.47	37.47	15.87
35.00	40.24	14.04	27.48	75.94	9.41	38.40	15.55
W 1.2 GeV ϕ = 8 cm							
5.00	17.82	8.81	10.57	32.93	4.68	17.19	8.91
20.00	20.01	9.09	21.11	80.12	2.67	19.92	9.13
34.75	19.61	9.13	7.78	93.24	0.00	19.75	8.93
W 1.2 GeV ϕ = 12 cm							
5.00	18.42	9.31	10.86	32.78	4.61	17.87	9.31
20.00	21.85	9.52	13.33	80.33	1.98	21.60	9.63
34.75	21.68	9.30	19.28	91.45	0.00	21.77	9.14
W 1.2 GeV ϕ = 15 cm							
1.00	15.11	6.78	8.75	6.83	2.24	13.30	7.68
2.00	16.33	7.86	9.69	13.58	3.80	14.75	8.47
5.00	18.70	9.50	9.70	33.06	4.61	17.93	9.54
10.00	21.29	9.85	10.27	54.29	5.28	20.38	10.18
15.00	22.49	9.63	12.40	67.27	5.30	21.59	10.15
20.00	22.83	9.53	14.22	77.21	3.67	22.27	9.91
25.00	22.75	9.40	28.88	82.64	2.93	22.47	9.67
30.00	22.69	9.40	17.94	88.39	0.00	22.69	9.35
34.75	22.49	9.30	13.26	90.46	0.00	22.56	9.16
W 1.8 GeV ϕ = 8 cm							
0.26	16.44	5.97	9.05	1.62	0.79	13.16	8.00
0.50	16.81	6.95	9.84	3.39	1.22	14.25	8.43
1.00	17.95	7.95	10.87	6.74	2.43	15.50	9.23
2.00	19.57	9.38	11.80	13.58	3.88	17.54	10.22
3.00	20.89	10.20	12.07	20.17	4.95	19.05	10.86

4.00	22.02	10.66	12.62	26.01	6.16	20.18	11.34
5.00	23.08	10.88	13.85	30.84	7.49	21.18	11.65
7.00	24.18	11.61	11.83	42.95	5.94	22.92	11.96
10.00	25.58	11.37	13.80	52.87	7.90	24.13	12.01
15.00	27.18	11.57	15.20	68.62	5.80	26.44	11.92
20.00	27.87	11.40	17.52	78.06	5.98	27.12	11.83
25.20	27.98	11.26	22.41	84.26	5.05	27.54	11.57
30.20	27.92	11.24	26.98	89.03	4.06	27.74	11.38
34.49	27.84	11.16	31.77	91.64	3.74	27.77	11.25
W 1.8 GeV ϕ = 12 cm							
20.00	30.71	11.95	18.39	77.73	5.91	29.86	12.53
24.00	31.03	11.76	17.46	84.35	4.48	30.34	12.22
30.00	31.02	11.66	32.27	88.04	4.07	30.76	11.88
34.49	30.95	11.59	25.45	92.11	2.15	30.81	11.66
W 1.8 GeV ϕ = 15 cm							
1.00	17.55	8.45	9.08	7.36	1.81	15.55	9.24
2.00	19.88	9.66	12.34	13.68	4.07	17.89	10.48
3.00	21.50	10.39	13.54	19.58	6.02	19.37	11.22
4.00	22.89	11.11	12.77	25.83	6.56	20.78	11.83
5.00	24.24	11.42	15.10	30.01	8.22	22.09	12.22
7.00	26.44	11.69	18.07	37.84	11.49	24.01	12.81
8.00	27.28	12.49	13.48	45.97	7.36	25.59	13.12
10.00	28.30	12.12	17.85	51.35	10.06	26.49	12.98
12.00	30.01	12.35	16.59	58.24	9.15	28.22	13.32
15.00	30.46	11.86	22.77	64.67	11.01	28.86	12.89
20.00	31.40	11.70	24.96	75.97	8.57	30.36	12.46
24.74	31.67	11.59	32.38	82.03	7.15	31.04	12.13
30.00	31.61	11.47	33.71	88.13	4.46	31.33	11.76

34.49	31.38	11.33	45.06	92.57	2.28	31.35	11.35
W 2.5 GeV $\phi = 8$ cm							
0.26	18.02	6.74	11.63	1.63	0.77	14.00	9.24
0.50	18.71	7.92	11.86	3.35	1.15	15.43	9.80
2.00	22.33	11.20	13.65	13.87	3.68	19.70	12.26
5.00	27.14	13.46	12.46	32.43	5.89	24.86	14.11
10.00	31.60	14.04	15.40	54.04	6.04	30.25	14.58
15.00	34.19	13.73	16.78	67.11	8.01	32.32	14.82
25.00	35.76	13.47	20.06	84.37	5.62	34.74	14.14
30.00	35.86	13.21	31.00	87.40	5.75	35.23	13.72
34.75	35.99	13.15	34.31	89.21	5.57	35.46	13.69
W 2.5 GeV $\phi = 12$ cm							
2.00	22.95	11.36	14.20	13.61	4.01	20.23	12.45
34.75	40.25	13.63	33.09	92.01	4.35	39.66	14.16
W 2.5 GeV $\phi = 15$ cm							
1.00	20.63	9.44	12.97	6.77	2.41	17.29	11.09
2.00	23.22	11.67	13.53	13.91	3.83	20.46	12.67
3.00	25.43	12.91	14.14	20.26	5.01	22.85	13.68
5.00	29.07	14.42	14.47	31.79	6.12	26.75	15.06
7.00	32.34	14.81	16.10	40.52	8.54	29.46	15.94
10.00	35.71	14.98	18.09	51.30	9.96	32.73	16.53
15.00	39.29	14.64	23.07	64.85	11.37	36.55	16.48
20.00	41.03	14.35	30.04	73.93	10.96	38.96	15.99
25.00	41.95	13.97	29.53	82.25	8.54	40.37	15.40
30.00	42.15	13.85	34.26	87.74	6.32	41.19	14.80
34.75	42.17	13.72	37.72	91.41	4.54	41.56	14.33
Hg 1.2 GeV $\phi = 15$ cm							

2.00	16.98	7.25	8.76	9.42	3.57	14.35	8.52
3.25	18.16	7.70	11.49	13.93	6.48	15.47	9.11
5.23	19.42	8.30	12.66	22.20	8.92	16.94	9.64
7.00	19.37	8.80	12.96	30.78	7.08	17.90	9.56
10.23	21.09	8.92	18.11	39.07	11.99	19.33	10.10
15.13	21.87	9.29	15.28	55.29	8.80	20.51	10.18
20.23	22.05	9.46	20.30	67.36	6.64	21.37	9.92
25.18	22.00	9.52	15.52	77.14	1.99	21.78	9.62
30.45	21.86	9.52	4.81	84.76	0.00	21.91	9.41
Hg 1.8 GeV $\phi = 15$ cm							
2.00	20.28	8.82	12.65	9.40	3.29	17.66	10.22
5.00	24.11	10.83	14.57	22.96	6.46	21.65	11.99
10.23	27.47	11.76	17.26	41.70	9.34	25.26	12.90
15.13	29.05	12.04	22.90	55.64	9.22	27.64	12.86
20.23	30.26	11.83	23.32	66.08	9.72	28.81	12.81
25.18	30.53	12.04	17.16	77.64	3.81	29.95	12.42
30.45	30.56	12.10	19.86	84.63	0.77	30.60	11.98
33.70	30.44	11.98	22.19	89.06	0.67	30.54	11.84
Hg 2.5 GeV $\phi = 15$ cm							
5.00	28.44	13.18	13.99	23.65	5.98	25.08	14.52
10.23	33.47	14.31	16.78	42.44	8.70	30.51	15.77
15.13	36.25	14.46	17.88	56.09	8.94	33.71	15.93
20.23	38.12	14.29	21.75	66.68	8.97	36.11	15.70
25.18	39.02	14.24	21.83	74.74	7.34	37.44	15.39
30.45	39.56	14.02	23.86	80.85	6.19	38.38	14.97
33.70	39.42	14.00	23.37	85.18	4.85	38.54	14.71